Frontiers in Bioscience Landmark

Front. Biosci. (Landmark Ed) **2026**; 31(6): 47735
https://doi.org/10.31083/FBL47735

Original Research

Huaier Sensitizes Oxaliplatin-Resistant Colorectal Cancer to Oxaliplatin by Reducing P-Glycoprotein and Inducing Nrf2/SLC7A11/GPX4-Dependent Ferroptosis

Guizhen Wang[1], Yanan Yuan[2], Hairu Ji[1], Xin Liu[3], Zhiping Hou[1], Jining Zheng[1,*]

[1]Department of Pathophysiology, Chengde Medical University, 067000 Chengde, Hebei, China
[2]Department of Histology and Embryology, Chengde Medical University, 067000 Chengde, Hebei, China
[3]Department of Oncology Chengde, Affiliated Hospital of Chengde Medical University, 067000 Chengde, Hebei, China
*Correspondence: cdyxyzjn@cdmc.edu.cn (Jining Zheng)
Academic Editor: Jordi Sastre-Serra
Submitted: 27 October 2025 Revised: 5 May 2026 Accepted: 9 May 2026 Published: 15 June 2026

Abstract

Background: Chemoresistance to oxaliplatin (OXA) in colorectal cancer (CRC) remains a major cause of treatment failure. This study investigated whether Huaier polysaccharide (HP) could reverse OXA resistance and explored the underlying mechanisms. **Methods**: Cell viability and proliferation were assessed using the Cell Counting Kit-8 (CCK-8) assay and colony formation assays, respectively. Protein expression was analyzed by Western blotting. Ferroptosis was evaluated using a lipid peroxidation probe (BDP 581/591 C11), FerroOrange, a reactive oxygen species (ROS) assay kit, and a total glutathione detection kit. Ultrastructural changes were observed using transmission electron microscopy. Nuclear and cytoplasmic protein extraction and immunofluorescence were used to examine nuclear factor erythroid 2-related factor 2 (Nrf2) expression. **Results**: Combined treatment with OXA and HP significantly suppressed cell viability and proliferation by inhibiting the Nrf2/solute carrier family 7 member 11 (SLC7A11)/glutathione peroxidase 4 (GPX4) pathway, thereby inducing ferroptosis. In addition, HP reduced P-glycoprotein expression and enhanced sensitivity to OXA. **Conclusions**: These findings demonstrate that Huaier overcomes OXA resistance in CRC cells by promoting ferroptosis through suppression of the Nrf2/SLC7A11/GPX4 signaling pathway *in vitro*.

Keywords: colorectal neoplasms; drug resistance; ferroptosis; Huaier; nuclear factor erythroid 2-related factor

1. Introduction

According to the GLOBOCAN 2022 data, colorectal cancer (CRC) represents a substantial global health burden. It ranks as the third most common malignancy in terms of incidence and the second leading cause of cancer-related mortality, underscoring its persistent public health impact [1]. Standard chemotherapeutic regimens for CRC comprise irinotecan, 5-fluorouracil, and oxaliplatin (OXA) [2]. As a third-generation platinum-based antitumor drug, OXA is recommended as the first-line standard treatment for metastatic CRC. Clinical recommendations are usually OXA-containing regimens, such as FOLFOX/CAPOX [3]. However, OXA resistance markedly compromises its clinical efficacy, with first-line response rates of only 20–24%, declining to approximately 10% in the second-line setting [4]. Therefore, overcoming OXA chemoresistance and improving treatment outcomes remain urgent priorities in CRC management.

Ferroptosis is an iron-dependent, non-apoptotic mechanism of cell death characterized by excessive lipid peroxidation. Its distinctive morphological and biochemical features include mitochondrial shrinkage, glutathione (GSH) depletion, and accumulation of aberrant lipid peroxidation products [5]. Accumulating evidence indicates that ferroptosis plays a critical role in the development of OXA resistance. Conversely, induction of ferroptosis has been shown to reverse chemoresistance in tumors, a finding that has attracted considerable attention in cancer research [6,7,8,9].

Nuclear factor erythroid 2-related factor 2 (Nrf2), originally identified as a key regulator of oxidative stress adaptation, is increasingly recognized as a critical driver of cancer progression, metastasis, and therapeutic resistance [10]. Emerging evidence suggests that Nrf2 promotes radiation-induced DNA damage repair via a reactive oxygen species (ROS)-independent homologous recombination pathway, thereby contributing to tumor cell resistance to radiotherapy and chemotherapy [11]. These findings imply that targeting Nrf2-mediated cellular defense pathways may reverse chemoresistance in cancer cells. Dysregulation of the solute carrier family 7 member 11–glutathione–glutathione peroxidase (SLC7A11/GSH/GPX4) axis represents a central mechanism conferring OXA resistance in multiple cancer types [9]. As one of the two subunits of System Xc^-, SLC7A11 is transcriptionally regulated by Nrf2 within the GSH metabolic pathway. Importantly, GPX4, a key enzyme that suppresses lipid peroxidation and regulates ferroptosis, is directly transcribed by Nrf2 [12]. Accordingly, we hypothesize that targeted inhibition of the Nrf2/SLC7A11/GPX4 signaling axis may effectively alleviate OXA resistance in CRC.

In recent years, natural medicines have attracted growing research interest, with traditional Chinese medicine (TCM) gaining broader recognition. Huaier (*Trametes robiniophila Murr*), a medicinal fungus that parasitizes the trunks of *Sophora japonica*, has been used in clinical practice in China for more than 1,600 years. Its primary active component is a proteoglycan composed of a heteropolysaccharide composed of six monosaccharides conjugated to a protein with a moiety of 18 amino acids [13]. Clinical evidence indicates that Huaier granules exert antitumor effects across multiple cancer types, including hepatocellular carcinoma [14], breast cancer [15], and CRC [16]. Moreover, Huaier has been used as an adjunct to conventional oncology to enhance chemosensitivity, reverse drug resistance, and reduce chemotherapy-related adverse effects. For example, Yang et al. [17] reported that Huaier extract enhances paclitaxel efficacy in breast cancer cells by regulating the NF-κB/IκBα signaling pathway. Similarly, Jin et al. [18] demonstrated that Huaier overcomes cisplatin resistance in non-small cell lung cancer cells by blocking the JNK/JUN/IL-8 signaling pathway. Despite these promising results, most studies have used Huaier granules or crude extracts, which contain substantial impurities and exhibit low polysaccharide purity, often requiring high concentrations to achieve therapeutic effects. Therefore, investigating the role of the primary active component, Huaier polysaccharide (HP), in CRC chemoresistance is of considerable scientific interest. This study aims to elucidate the mechanism by which HP suppresses drug resistance in CRC.

In this study, we investigated the effects of HP on OXA resistance in CRC and explored the underlying mechanisms. Our *in vitro* findings demonstrated that HP sensitizes CRC cells to OXA by suppressing the Nrf2/SLC7A11/GPX4 signaling axis, thereby inducing ferroptosis. Collectively, these results provide experimental evidence supporting the potential of combining Huaier with OXA to overcome OXA chemoresistance in CRC cells.

2. Materials and Methods

2.1 Chemicals

HP was purchased from Yuanye Biotechnology Co., Ltd. (catalog no. S28138; LOT: C02J11Y106867), dissolved in RPMI-1640 medium (Procell Life Science & Technology Co., Ltd., Wuhan, China), and sterilized using a 0.22-μm filter (Merck Millipore, Darmstadt, Germany). HP with a purity of 60.7% was extracted using a water extraction and alcohol precipitation method. Chemical analysis of HP has shown that it contains 60.7% total polysaccharides, 1.85% flavonoids, 3.57% phenolic acids, and 0.12% total protein. Gel Permeation Chromatography (GPC) results indicated that the average molecular weight (Mw) of HP was 11.114 kDa [19]. Further studies have reported that HP consists of 41.5% carbohydrates, 12.93% amino acids (Asp, Thr, Ser, Glu, Pro, Gly, Ala, Cys, Val, Met, Ile, Leu, Tyr, Phe, Lys, His, Trp, and Arg), and 8.72% moisture, as well as six constituent monosaccharides: fucose, arabinose, xylose, mannose, galactose, and glucose [20]. Wang et al. [21] isolated a polysaccharide with a purity of 85.3 ± 1.3%, with the same six monosaccharides present at molar percentages of 5.82%, 13.11%, 16.88%, 15.85%, 11.40%, and 36.94%, respectively.

2.2 Cell Lines and Culture

HCT116 (cat. no. MXC151) and resistant HCT116/L cells (cat. no. MXC469) were purchased from MEIXUAN Biological Science and Technology, Ltd. (Shanghai, China). HCT8 cells (cat. no. PC193) were obtained from Procell Life Science & Technology Co., Ltd. Oxaliplatin-resistant HCT8/L cells were obtained from Shanghai Aolu Biotechnology. HCT116/L and HCT8/L cells were generated by exposing parental cells to a protocol involving gradually increasing concentrations of OXA with intermittent high-dose drug pulses. All cell lines were cultured in RPMI-1640 medium supplemented with 10% fetal bovine serum (Procell Life Science & Technology Co., Ltd.). To maintain the drug-resistant phenotype, HCT116/L cells were cultured in medium containing 2000 ng/mL OXA, whereas HCT8/L cells were maintained in medium containing 1000 ng/mL OXA. All cells were incubated at 37 °C in a 5% CO_2 incubator. All cell lines used in this study (including HCT116, HCT116/L, HCT8, HCT8/L) were maintained in culture for no more than 10 passages after thawing. The cell lines were validated by short tandem repeat profiling and tested negative for *Mycoplasma* species.

2.3 Cell Viability Assay

Cell viability was assessed using a Cell Counting Kit-8 (CCK-8) assay (cat. no. K1018; APeXBIO Technology LLC, Shanghai, China). Cells were seeded in a 96-well plate at 2000–4000 cells/well and cultured overnight under standard conditions (37 °C, 5% CO_2). Next, they were exposed to varying concentrations of OXA or HP for 48 h. Subsequent cell viability was assessed using a CCK-8 assay, wherein a mixture of 10 μL of CCK-8 reagent and 100 μL of RPMI-1640 medium was added to each well. After a 2-h incubation in the dark at 37 °C, the absorbance at 450 nm was measured with a microplate reader. Cell viability was derived from the formula: [(As – Ab) / (Ac – Ab)] × 100%, with As, Ac, and Ab representing the absorbance values of the sample, control, and blank groups, respectively. The resistance index (RI) was calculated as: RI = IC_{50} (resistant cells)/IC_{50} (parental cells).

2.4 Colony Formation Assays

To evaluate clonogenic ability, cells were seeded at a density of 800 cells per dish in 3.5-cm culture dishes and cultured under standard conditions (37 °C, 5% CO_2) for 4 days. The medium was then replaced with a drug-containing medium for 48 h. After treatment, the cells were washed with PBS and cultured in fresh drug-free medium

until visible colonies formed. The supernatant was discarded and the cells were washed once with PBS, fixed with 4% paraformaldehyde (Biosharp, Hefei, China) for 30 min, and washed again with PBS. The colonies were stained with crystal violet solution (Solarbio Life Sciences) for 15 min, at which time excess dye was removed by gentle rinsing with water. The dishes were air-dried and imaged, and the number of colonies was quantified using ImageJ software (version 5.2.1; Bio-Rad Laboratories, Inc., Hercules, CA, USA).

2.5 Transmission Electron Microscopy

Image analysis of ferroptosis was performed by Servicebio (cat. no. GP2075; Wuhan Servicebio Technology CO., Ltd., Wuhan, China). In brief, the experimental procedure comprised the following steps: harvest samples and fixation, agarose pre-embedding, post-fixation, dehydration at room temperature, resin penetration and embedding, polymerization, ultrathin sectioning, staining and observation, and image capture.

2.6 Lipid Peroxidation Assessment

A BODIPY 581/591 C11 (cat. no. L267; Dojindo Molecular Technologies, Inc., Japan) was used to measure intracellular lipid peroxidation. The assay was performed according to the manufacturer's instructions. The cells were seeded in 24-well plates (4×10^4 cells/well). After overnight cultivation at 37 °C and 5% CO_2, both resistant cell lines were treated with HP, OXA, or their combination (with or without Fer-1 or TBHQ) for 48 h. The supernatant was removed and the cells were washed twice with PBS. BDP 581/591 C11 working solution was added, followed by incubation at 37 °C under 5% CO_2 for 30 min. The supernatant was removed, the cells washed twice with PBS, PBS added, and fluorescence detected using an inverted fluorescence microscope (Olympus Corporation). A quantitative analysis was performed using ImageJ software (version 5.2.1; Bio-Rad Laboratories, Inc.).

2.7 Intracellular Iron Assay

FerroOrange probes (cat. no. F374; Dojindo Molecular Technologies, Inc.) were used to measure cellular ferrous iron levels. The assay was performed according to the manufacturer's instructions. Briefly, cells were seeded in 24-well plates (4×10^4 cells/well) for 24 h, followed by treatment with HP, OXA, or their combination (with or without Fer-1 or TBHQ) for 48 h. Subsequently, after two PBS washes, the cells were stained with 1 μmol/L FerroOrange for 30 min and examined under an inverted fluorescent microscope (Olympus Corporation). A quantitative analysis was performed using ImageJ software (version 5.2.1; Bio-Rad Laboratories, Inc.).

2.8 ROS Assay

A ROS assay kit (cat. no. R252; Dojindo Molecular Technologies, Inc.) was used to measure ROS levels. The assay was performed according to manufacturer's instructions. Cells were seeded in 24-well plates at a density of 3×10^4 cells per well and incubated for 24 h prior to treatment. The cells were then treated with HP, OXA, or a combination thereof (with or without Fer-1 or TBHQ) for 48 h. A working ROS solution was prepared by diluting the highly sensitive 2′,7′-dichlorodihydrofluorescein diacetate dye 1000-fold in a loading buffer solution. After being washed twice with PBS, the cells were incubated with the ROS working solution at 37 °C under 5% CO_2 for 30 min. Fluorescence signals were observed using an inverted fluorescence microscope (Olympus Corporation), and a quantitative analysis of fluorescence intensity was performed using ImageJ software (version 5.2.1; Bio-Rad Laboratories, Inc.).

2.9 GSH Assay

A total GSH assay kit (cat. no. S0052; Beyotime Biotechnology, Shanghai, China) was used to determine total GSH content according to the manufacturer's instructions. At 48 h after the drug treatment, the cells were processed according to the manufacturer's instructions and their absorbance measured at 412 nm using a microplate reader.

2.10 Western Blot Analysis

The cells were lysed using RIPA lysis buffer (Report Biotech) supplemented with phenylmethylsulfonyl fluoride (PMSF; Coolaber, Beijing, China). Protein concentrations were quantified using a bicinchoninic protein assay kit (cat. no. KGB2101-500; KeyGEN, Jiangsu, China). The proteins (30 μg) were separated on 10–12% sodium dodecyl sulfate–polyacrylamide gel electrophoresis gels according to their molecular weights and transferred onto polyvinylidene fluoride membranes. The membranes were blocked with 5% skim milk (Solarbio Life Sciences) for 2 h at room temperature and incubated overnight at 4 °C on a shaker with the following primary antibodies: p-glycoprotein (P-gp; 1:1000; cat. no. 13978; Cell Signaling Technology, Inc., Danvers, MA, USA) and Nrf2 (1:3000; cat. no. 80593-1-RR; Proteintech Group, Inc., Shanghai, China), and GPX4 (1:1000; cat. no. A11243; ABclonal Biotech Co., Ltd., China) and SLC7A11 (1:1000; cat. no. A2413; ABclonal Biotech Co., Ltd., China), and H3 (1:2000; cat. no. bsm-33042R; BIOSS, China), glyceraldehyde-3-phosphate dehydrogenase (1:10,000; cat. no. bsm-52262R; BIOSS), and β-actin (1:50,000; cat. no. AC026; ABclonal Biotech Co., Ltd., China). After being washed, the membrane was incubated with goat anti-rabbit IgG (H+L) secondary antibody (1:10,000; cat. no. RGAR001; Proteintech Group, Inc.) for 1 h at room temperature. Finally, the protein bands were visualized using an enhanced chemiluminescence reagent (Biosharp) and

imaged using a gel documentation system. The gray values of the protein bands were analyzed using ImageJ software (version 5.2.1; Bio-Rad Laboratories, Inc.). Band gray values were normalized to GAPDH/β-actin, and quantitative analysis was conducted using ImageJ software. Fluorescence intensity was quantified via ImageJ and normalized to the control group.

2.11 Immunofluorescence

The treated cells were washed once with PBS and fixed with 4% paraformaldehyde at room temperature for 15 min. After permeabilization with 0.1% Triton X-100 (Solarbio Life Sciences) at 4 °C for 15 min, the cells were washed three times with PBS. Subsequently, the sections were blocked with 2% bovine serum albumin (Solarbio Life Sciences) at room temperature for 2 h and incubated with an anti-Nrf2 antibody (1:300; cat. no. 80593-1-RR; Proteintech Group, Inc.) overnight at 4 °C. After three washes with PBS, the cells were incubated with goat anti-rabbit IgG labeled with RGAR004 - Multi-rAb® CoraLite® Plus 594-Goat Anti-Rabbit Recombinant Secondary Antibody (H+L) (1:600; cat. no. RGAR004; Proteintech Group, Inc.) for 1 h at room temperature in the dark and washed three times with PBS. The nuclei were stained with 4′,6-diamidino-2-phenylindole (Coolaber) for 5 min, followed by three additional PBS washes. Imaging was performed immediately using a fluorescence microscope (Olympus). Finally, the mean fluorescence intensity was analyzed using ImageJ software (version 5.2.1; Bio-Rad Laboratories, Inc.).

2.12 Nuclear and Cytoplasmic Protein Extraction Kit

Nuclear and cytoplasmic proteins were extracted using nuclear and cytoplasmic protein extraction kits (cat. no. P0028; Beyotime Biotechnology). The assay was performed according to manufacturer's instructions. Briefly, the cells were washed once with PBS, scraped with a cell scraper, and collected by centrifugation. The resulting cell pellet was retained for the subsequent steps. To extract cytoplasmic proteins, 200 µL of Cytoplasmic Protein Extraction Reagent A, supplemented with PMSF, was added to the pellet. The mixture was vortexed vigorously at the maximum speed for 5 s and incubated on ice for 15 min. Next, 10 µL of Cytoplasmic Protein Extraction Reagent B was added, followed by vortexing at maximum speed for 5 s and incubation on ice for 1 min. After another 5-s vortex at maximum speed, the sample was centrifuged at 12,000–16,000 ×*g* for 5 min at 4 °C. The supernatant containing the cytoplasmic protein fraction was immediately collected. For nuclear protein extraction, 50 µL of Nuclear Protein Extraction Reagent supplemented with PMSF was added to the remaining pellet. The mixture was vortexed vigorously at the maximum speed for 30 s to fully suspend and disperse the pellet, followed by incubation on ice. The vortexing step (30 s at maximum speed) was repeated every 2 min for a total duration of 30 min. Finally, the sample was centrifuged at 16,000 ×*g* for 10 min at 4 °C, and the supernatant containing the nuclear protein fraction was collected.

2.13 Statistical Analysis

All data are presented as mean ± standard deviation. Intergroup comparisons were performed using Student's *t*-test, whereas comparisons among multiple groups were performed using one-way analysis of variance. Data analyses were conducted using SPSS version 20 (SPSS, Cary, NC, USA) and GraphPad Prism 8 (GraphPad, San Diego, CA, USA). Values of $p < 0.05$ were considered statistically significant, and ns denotes non-significance.

3. Results

3.1 HP Inhibited Cell Viability and Proliferation in Resistant Cell Lines and Exhibited Synergistic Effects With OXA

After 48 h of treatment with varying concentrations of OXA, cell viability in parental and resistant cells was assessed using the Cell Counting Kit-8 (CCK-8) assay, and the half-maximal inhibitory concentration (IC_{50}) values were calculated. The IC_{50} values for HCT116 and HCT116/L cells were 0.8021 µg/mL and 9.659 µg/mL, respectively, yielding an RI of 12.04, indicating marked drug resistance in HCT116/L cells (Fig. 1A). Similarly, the IC_{50} values of OXA in HCT8 and HCT8/L cells were 4.234 µg/mL and 13.18 µg/mL, respectively, corresponding to an RI of 3.11 (Fig. 1A). Treatment with different concentrations of HP for 48 h reduced the viability of HCT116/L and HCT8/L cells in a concentration-dependent manner (Fig. 1B). To evaluate the synergistic effects, HCT116/L and HCT8/L cells were treated with combinations of OXA and HP at various concentrations for 48 h. Cell viability was assessed using the CCK-8 assay, and the combination index (CI) was calculated using Compusyn software. Most CI values were <1 in both cell lines, indicating a synergistic effect between OXA and HP (Fig. 1C). Based on the cytotoxicity profiles, subsequent experiments were performed using 8 µg/mL OXA (approximately IC_{50}) and 700 µg/mL HP (approximately IC_{20}) for HCT116/L cells, and 13 µg/mL OXA and 700 µg/mL HP for HCT8/L cells, with all treatments lasting 48 h. Colony formation assays further confirmed that HP suppressed the proliferation of HCT116/L and HCT8/L and exhibited synergistic effects with OXA (Fig. 1D). Collectively, these results indicate that HP enhances the inhibitory effects of OXA on the viability and proliferation of drug-resistant CRC cells.

3.2 HP Enhances the Sensitivity of Colorectal Cancer Drug-Resistant Cells to OXA and Suppresses P-gp Expression

Comparison of the IC_{50} values between OXA alone and OXA combined with HP (700 µg/mL) in HCT116/L and HCT8/L cells revealed a significant decrease in IC_{50}

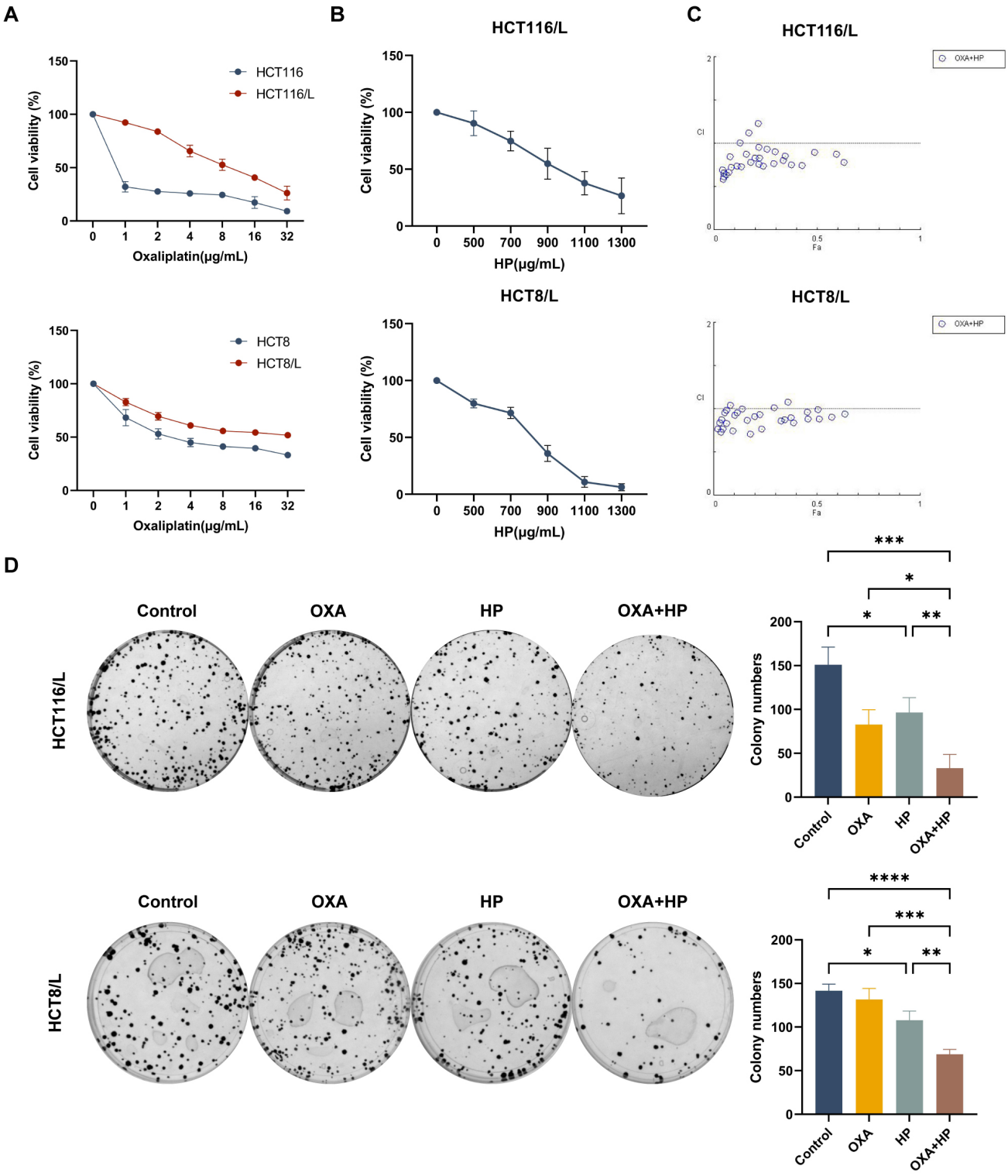

Fig. 1. Huaier polysaccharide (HP) inhibited the viability and proliferative capacity of colorectal cancer drug-resistant cells and exhibited a synergistic effect with oxaliplatin (OXA). (A) Survival rates of HCT116, HCT116/L, HCT8, and HCT8/L cells treated with different concentrations of OXA for 48 h as measured by a Cell Counting Kit-8 (CCK-8) assay. (B) Survival rates of HCT116/L and HCT8/L cells treated with varying concentrations of HP for 48 h as determined by a CCK-8 assay. (C) The combination index (CI) was calculated using Compusyn software. (D) Proliferative capacity of HCT116/L and HCT8/L cells treated with OXA alone, HP alone, or their combination was evaluated by a colony formation assay. Data are expressed as mean ± standard deviation. All experiments were performed with three independent biological replicates (n = 3). *$p < 0.05$, **$p < 0.01$, ***$p < 0.001$, and ****$p < 0.0001$.

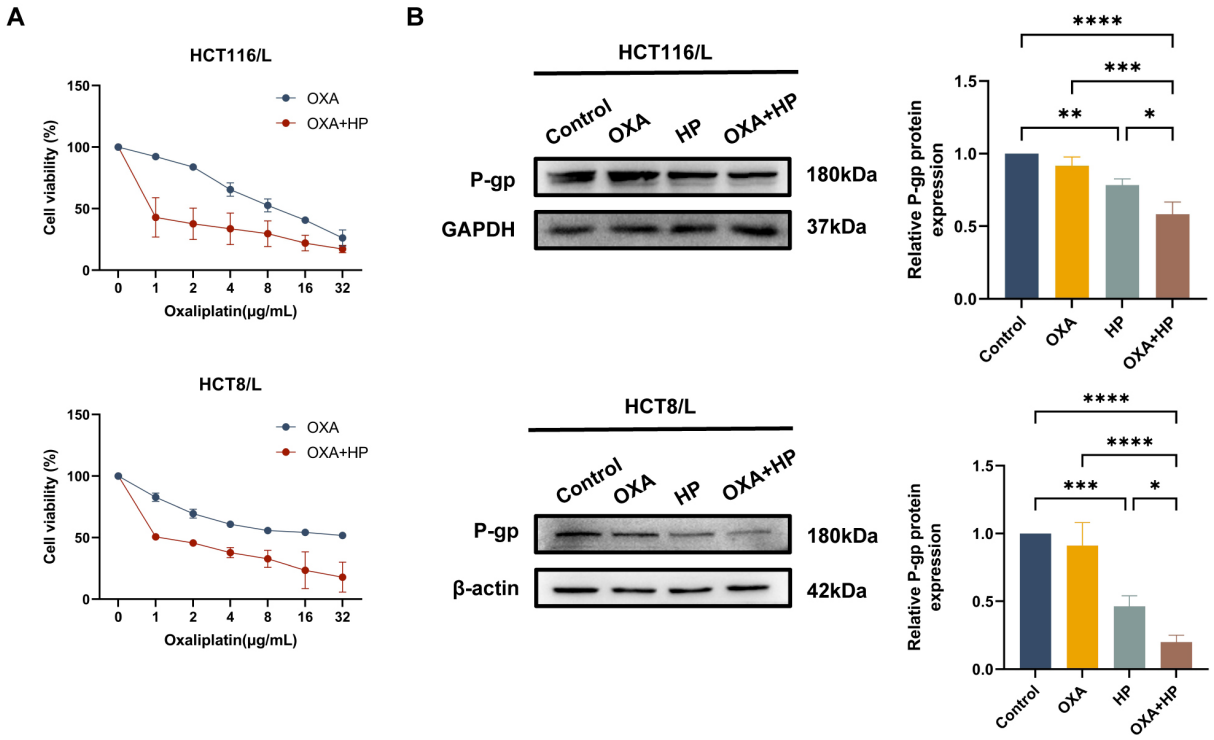

Fig. 2. Huaier polysaccharide (HP) enhanced the sensitivity of colorectal cancer drug-resistant cells to oxaliplatin (OXA) and suppressed p-glycoprotein (P-gp) expression. (A) Comparison of the IC_{50} values of OXA alone versus the OXA–HP combination in HCT116/L and HCT8/L cells. (B) P-gp expression levels in HCT116/L and HCT8/L cells treated with OXA alone, HP alone, or their combination as detected by western blotting. Data are expressed as mean ± standard deviation (n = 3). *$p < 0.05$, **$p < 0.01$, ***$p < 0.001$, and ****$p < 0.0001$.

following co-treatment, indicating that HP sensitizes drug-resistant CRC cells to OXA (Fig. 2A). Given that P-gp is widely recognized as a marker of chemoresistance, its protein expression was evaluated by Western blotting. HP reduced P-gp expression in drug-resistant cells, with a more pronounced effect when combined with OXA, suggesting that HP suppresses CRC chemoresistance (Fig. 2B). Collectively, these findings indicate that HP enhanced the sensitivity of drug-resistant CRC cells to OXA.

3.3 Chemoresistance in CRC Cells Is Associated With Ferroptosis

To further investigate whether chemoresistance in CRC was associated with ferroptosis, lipid peroxidation in HCT116, HCT8, HCT116/L, and HCT8/L cells was assessed using the BODIPY 581/591 C11 fluorescent probe (Fig. 3A). Intracellular Fe^{2+} levels were measured using FerroOrange (Fig. 3B), intracellular ROS levels were detected using an ROS assay kit (Fig. 3C), and total GSH content was quantified using a GSH assay kit (Fig. 3D). Compared with parental cells, drug-resistant cells exhibited reduced lipid peroxidation, lower Fe^{2+} levels, decreased ROS levels, and increased GSH content. These findings demonstrated that chemoresistance in CRC cells is linked to ferroptosis, with drug-resistant cells exhibiting relatively lower levels of ferroptosis.

3.4 HP Induced Ferroptosis in Colorectal Cancer Drug-Resistant Cells

Ultrastructural changes in drug-resistant cells following treatment with HP and OXA were examined using TEM. In the control group, mitochondria were predominantly oval in shape, with normal volume, intact cristae, and continuous membranes. Cells in the OXA group showed mild damage, with mitochondria largely retaining an oval morphology, normal volume, and intact membranes, but displaying slight matrix rarefaction. In the HP group, moderate damage was observed, characterized by features consistent with ferroptosis, including mitochondrial shrinkage, reduced volume, increased electron density, elevated membrane density, disrupted and diminished cristae, and the presence of autolysosomes. The combination treatment group exhibited more severe damage, with pronounced ferroptotic features such as marked mitochondrial shrinkage, volume reduction, condensation, increased membrane density, expanded and reduced cristae, and abundant autolysosome formation. TEM provided direct morphological evidence that HP induces ferroptosis in drug-resistant cells (Fig. 4A).

Subsequently, ferroptosis in HP-treated resistant cells was evaluated using the BODIPY 581/591 C11 fluorescent probe, FerroOrange, a ROS assay kit, and a total GSH assay

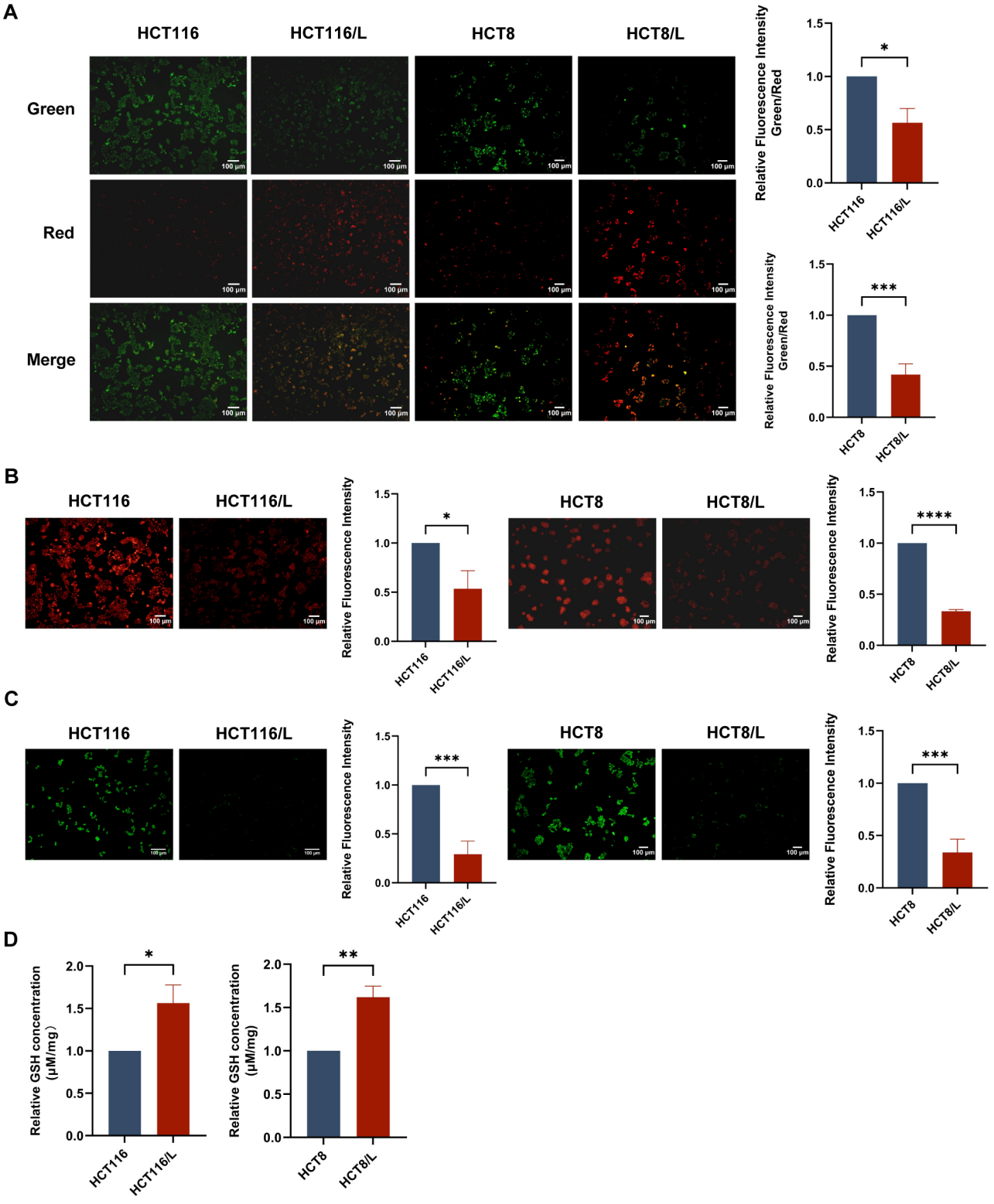

Fig. 3. Chemoresistance in colorectal cancer (CRC) cells is associated with ferroptosis. (A) Lipid peroxide formation in HCT116, HCT8, HCT116/L, and HCT8/L cells was assessed using the BODIPY 581/591 C11 fluorescent probe. Scale bar, 100 μm. (B) Intracellular Fe^{2+} levels were measured in HCT116, HCT8, HCT116/L, and HCT8/L cells using FerroOrange. Scale bar, 100 μm. (C) Reactive oxygen species (ROS) content was determined in HCT116, HCT8, HCT116/L, and HCT8/L cells using a ROS assay kit. Scale bar, 100 μm. (D) Total glutathione (GSH) content in parental (HCT116, HCT8) and drug-resistant (HCT116/L, HCT8/L) cells was quantified using a GSH assay kit. Data are expressed as mean ± standard deviation (n = 3). *$p < 0.05$, **$p < 0.01$, ***$p < 0.001$, and ****$p < 0.0001$.

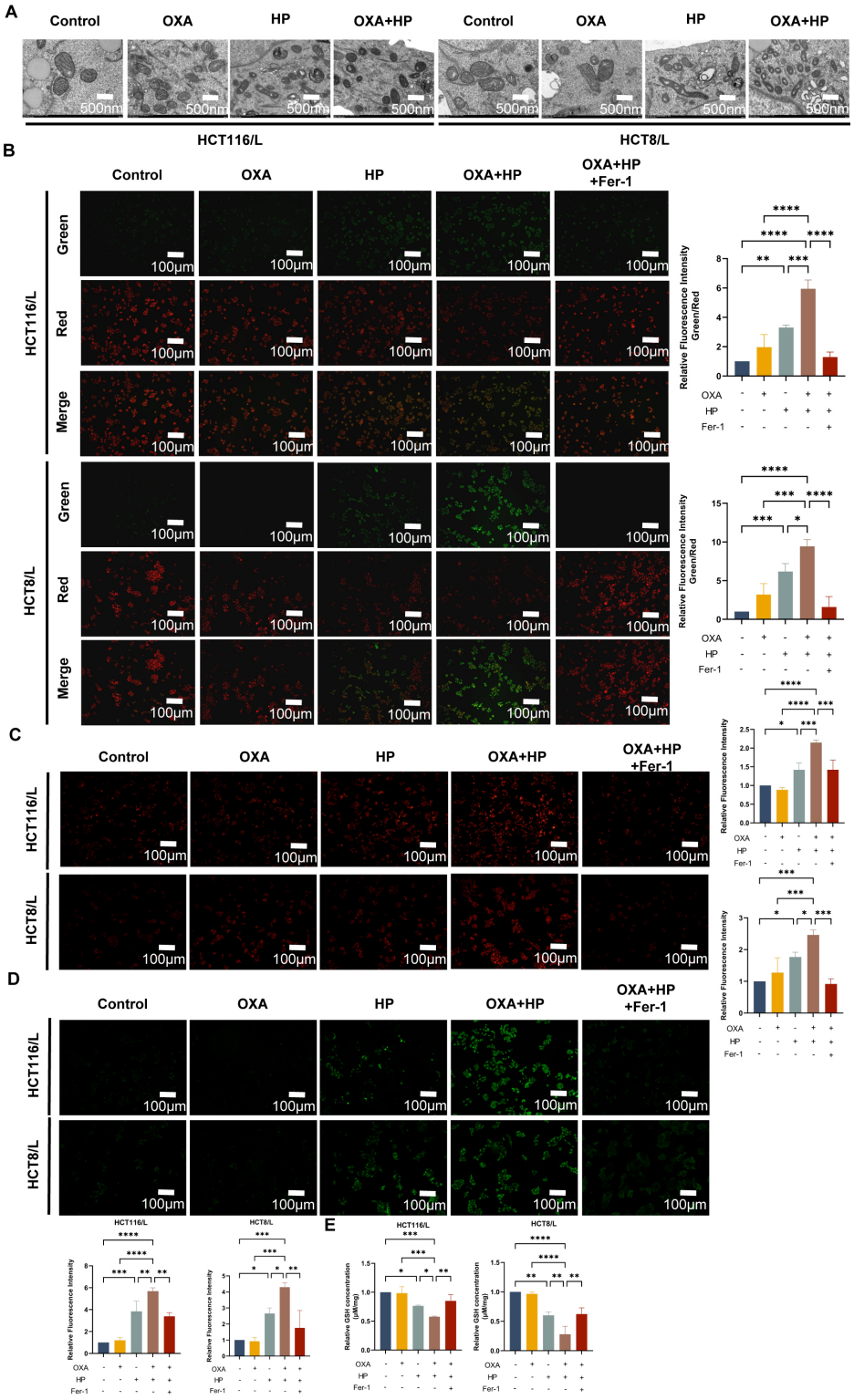

Fig. 4. Huaier polysaccharide (HP) induces ferroptosis in colorectal cancer drug-resistant cells. (A) Ultrastructural morphology of HCT116/L and HCT8/L cells after HP treatment was observed by transmission electron microscopy. Scale bar, 500 nm. (B) Lipid peroxidation was detected using the BODIPY 581/591 C11 fluorescent probe. Scale bar, 100 μm. (C) Intracellular Fe^{2+} levels were assessed using FerroOrange. Scale bar, 100 μm. (D) Reactive oxygen species (ROS) levels were measured using a ROS assay kit. Scale bar, 100 μm. (E) Total glutathione (GSH) content was measured with a GSH assay kit. Data are expressed as mean ± standard deviation (n = 3). *$p < 0.05$, **$p < 0.01$, ***$p < 0.001$, and ****$p < 0.0001$.

kit. HP increased lipid peroxidation (Fig. 4B), elevated intracellular Fe^{2+} levels (Fig. 4C), increased ROS levels (Fig. 4D), and reduced GSH content (Fig. 4E). Treatment with Fer-1 partially reversed these effects. Collectively, these findings demonstrate that HP induces ferroptosis in drug-resistant colorectal cancer cells.

3.5 HP Enhances the Sensitivity of Colorectal Cancer Drug-Resistant Cells to OXA by Inducing Ferroptosis

To confirm that HP mediates OXA chemosensitization through the regulation of ferroptosis, rescue experiments were performed using Fer-1. Following treatment with the combination of OXA and HP, cell viability was compared in the presence or absence of Fer-1. The inhibitory effects of OXA and HP on drug-resistant cells were partially reversed by Fer-1 treatment (Fig. 5A). Similarly, Western blot analysis demonstrated that the suppression of p-glycoprotein expression was partially reversed by Fer-1 (Fig. 5B). Consistent results were obtained in the colony formation assay (Fig. 5C). Collectively, these findings indicate that HP enhances the sensitivity of oxaliplatin-resistant colorectal cancer cells to OXA by inducing ferroptosis.

3.6 HP Inhibits Nrf2/SLC7A11/GPX4 Signaling Pathway

To determine whether HP affected the Nrf2/SLC7A11/GPX4 pathway, drug-resistant colorectal cancer cells were treated with OXA, HP, or their combination. Western blot analysis showed that the protein expression levels of Nrf2, SLC7A11, and GPX4 were downregulated under all treatment conditions, with the greatest reduction observed in the combination treatment group (Fig. 6A). To further assess whether HP influences Nrf2 nuclear and cytoplasmic translocation, nuclear–cytoplasmic fractionation (Fig. 6B) and immunofluorescence assays (Fig. 6C) were performed. HP suppressed Nrf2 expression in the nucleus and cytoplasm, whereas the combination treatment exerted stronger inhibitory effects than either agent alone. Collectively, these findings indicated that HP effectively inhibited the Nrf2/SLC7A11/GPX4 pathway.

3.7 HP Enhances OXA Sensitivity by Inducing Ferroptosis via Inhibiting Nrf2/SLC7A11/GPX4 Pathway

To confirm that HP specifically regulates ferroptosis and chemosensitivity via the Nrf2/SLC7A11/GPX4 signaling axis, functional validation was performed using the Nrf2 activator TBHQ. After treating drug-resistant colorectal cancer cells with OXA and HP, pathway-related protein expression levels were compared in the presence or absence of TBHQ. Western blot analysis showed that HP-induced suppression of Nrf2, SLC7A11, and GPX4 protein expression was partially reversed by TBHQ treatment (Fig. 7A). Consistent results were observed in nuclear–cytoplasmic fractionation and immunofluorescence assays, in which TBHQ restored HP-inhibited Nrf2 protein expression (Fig. 7B,C). To further determine whether HP modulates ferroptosis via the Nrf2 pathway, lipid peroxidation, intracellular Fe^{2+} levels, ROS levels, and GSH content—key indicators of ferroptosis—were evaluated in drug-resistant colorectal cancer cells using the BODIPY 581/591 C11 probe, FerroOrange, an ROS assay kit, and a total GSH assay kit, respectively. HP increased lipid peroxidation (Fig. 7D), and this effect was attenuated by TBHQ. Similar trends were observed for Fe^{2+} levels, ROS levels, and total GSH content (Fig. 7E–G), supporting the role of the Nrf2 pathway in ferroptosis. Next, we investigated whether HP affected OXA sensitivity in colorectal cancer drug-resistant cells via the Nrf2/SLC7A11/GPX4 axis. The CCK-8 assay revealed that TBHQ partially reversed HP-mediated suppression of cell viability (Fig. 7H). The colony formation assay yielded consistent results, and Western blot analysis showed that the combination of OXA and HP with TBHQ increased P-gp expression (Fig. 7I,J). Collectively, these findings indicate that HP increases OXA sensitivity by suppressing the Nrf2/SLC7A11/GPX4 signaling pathway and inducing ferroptosis.

4. Discussion

CRC is among the most common malignancies worldwide [22]. Over the past decade, OXA resistance has become a major obstacle in the clinical treatment of CRC, thereby limiting its therapeutic efficacy [23]. Therefore, improving the sensitivity of CRC to OXA chemotherapy is essential for enhancing treatment outcomes.

A growing body of research indicates that modulation of ferroptosis can significantly enhance chemosensitivity in CRC. For example, Li et al. [7] reported that *Fusobacterium nucleatum* suppresses ferroptosis via the E-cadherin/β-catenin/GPX4 axis, thereby promoting OXA resistance in CRC. Similarly, Yang et al. [24] demonstrated that the circadian rhythm gene, ARNTL2, upregulates SLC7A11 and inhibits ferroptosis, leading to CRC resistance to 5-fluorouracil in CRC cells. In the present study, ferroptosis in parental and resistant cell lines was evaluated using the BODIPY 581/591 C11 fluorescent probe, FerroOrange fluorescent probe, an ROS assay kit, and a total GSH assay kit. These results are consistent with previous findings, indicating that the drug-resistant phenotype of CRC cells is closely associated with ferroptosis, with resistant cells exhibiting lower levels of ferroptotic activity.

In recent years, TCM has attracted increasing attention because of its multi-target properties, potential to reduce adverse effects, and ability to act synergistically with conventional chemotherapy. For instance, curcumin inhibits tumor progression by targeting colorectal adenomas and cancer stem cells [25], whereas Gegen Qinlian Decoction improves OXA resistance by suppressing YTHDF1-mediated m6A modification of GLS1 [26]. Huaier (*Trametes robiniophila Murr*), a medicinal fungus that grows on aged *Sophora japonica* trees, has demonstrated therapeu-

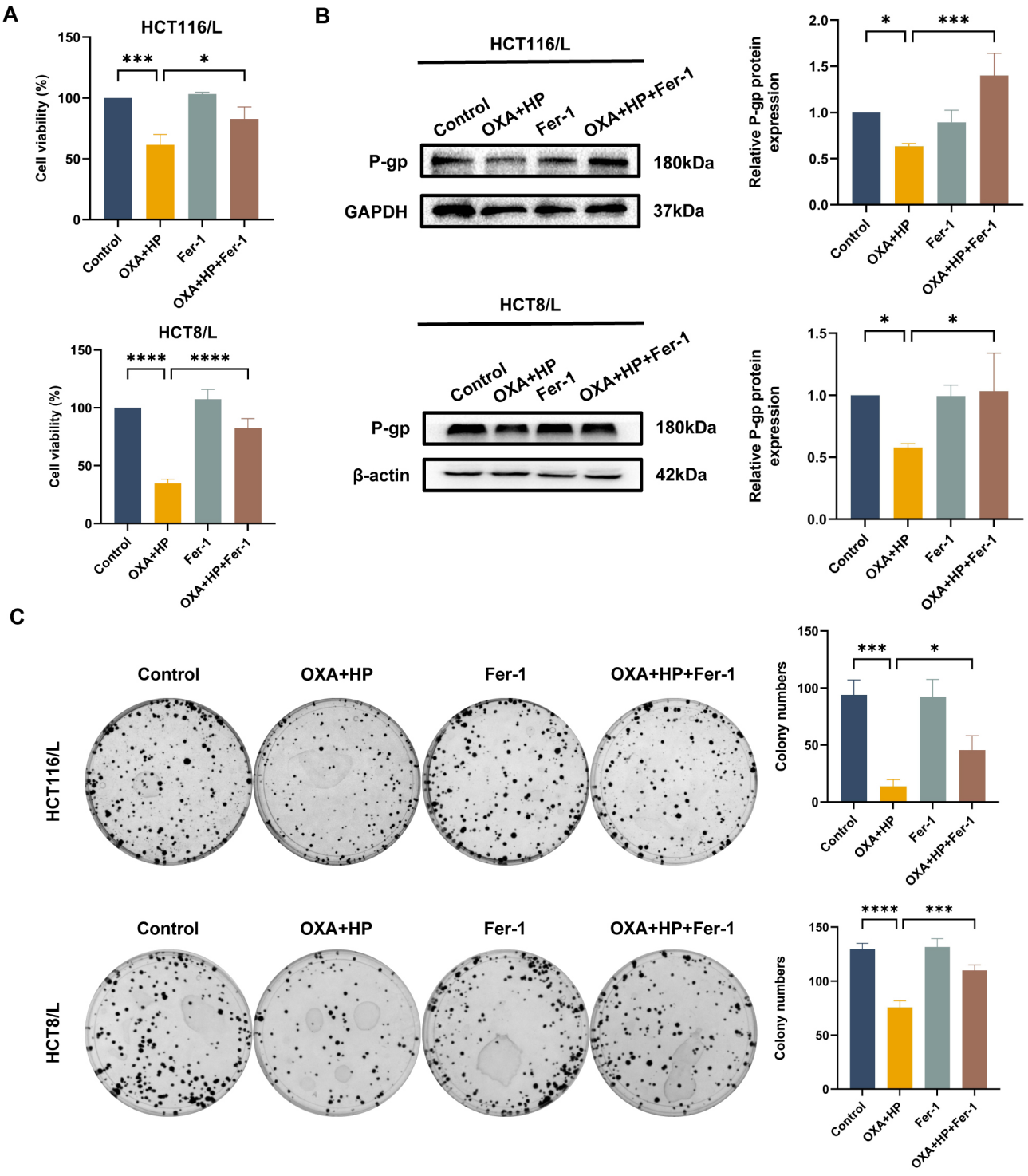

Fig. 5. Huaier polysaccharide (HP) enhances the sensitivity of colorectal drug-resistant cells to oxaliplatin (OXA) by inducing ferroptosis. (A) Cell viability of colorectal drug-resistant cells treated with OXA combined with HP, with or without the addition of ferrostatin-1 (Fer-1), was detected using a Cell Counting Kit-8 assay. (B) P-glycoprotein expression levels in colorectal drug-resistant cells treated with OXA combined with HP, with or without Fer-1, were measured by western blotting. (C) Colony formation ability of colorectal drug-resistant cells treated with OXA combined with HP, with or without Fer-1, was assessed (n = 3). Data are expressed as mean ± standard deviation; *$p < 0.05$, ***$p < 0.001$, and ****$p < 0.0001$.

tic efficacy against various malignancies, including liver, lung, breast, and gastric cancers, and inhibits tumor growth and metastasis through multiple pathways [27]. Recent studies have shown that Huaier enhances the sensitivity of

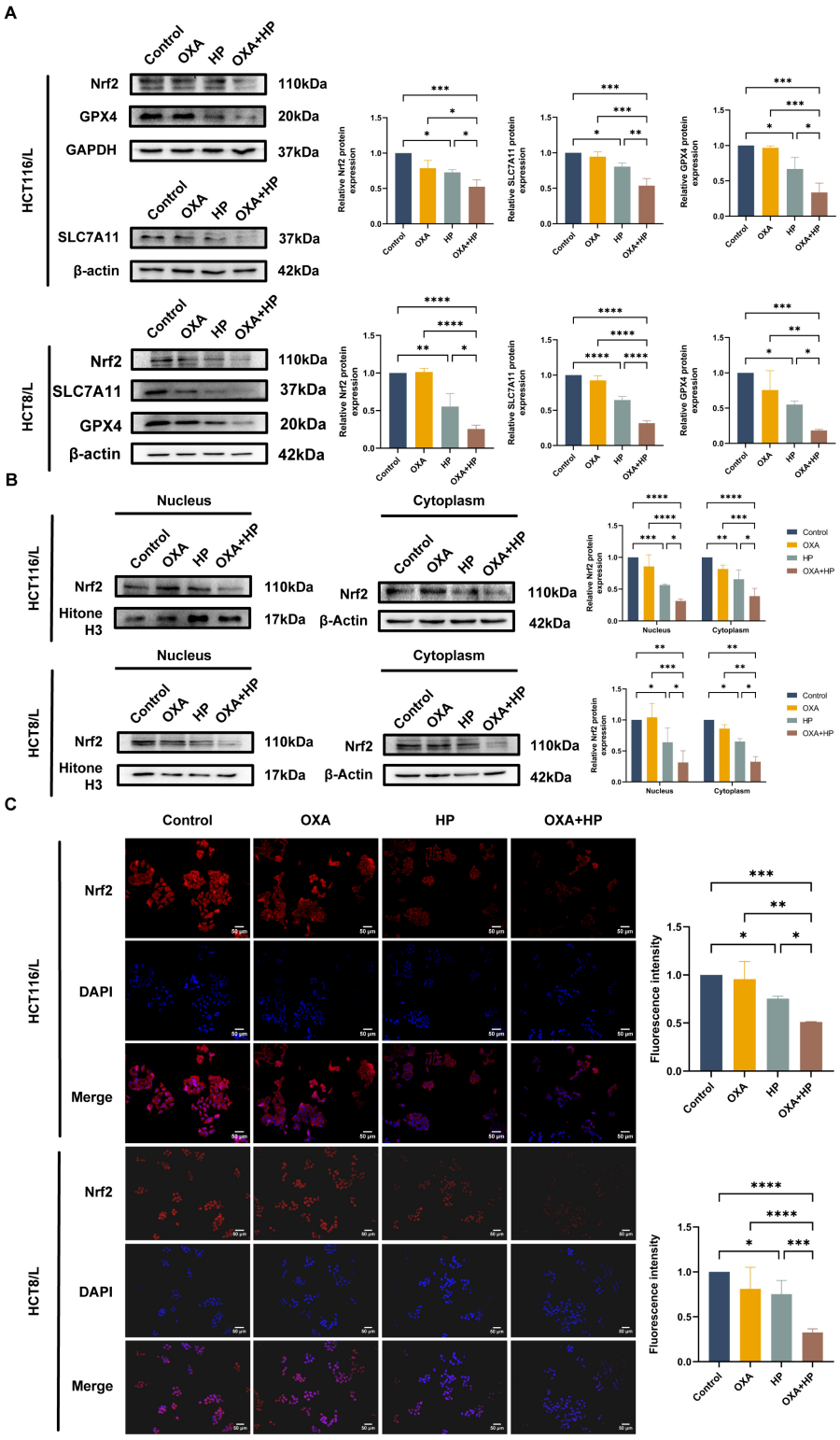

Fig. 6. Huaier polysaccharide (HP) inhibits the nuclear factor erythroid 2-related factor 2/solute carrier family 7 member 11/glutathione peroxidase (Nrf2/SLC7A11/GPX4) signaling pathway. (A) Protein expression levels of Nrf2, SLC7A11, and GPX4 in colorectal cancer drug-resistant cells after co-treatment with oxaliplatin (OXA) and HP were detected by western blotting. (B) Nuclear and cytoplasmic distribution of Nrf2 protein was analyzed using nuclear–cytoplasmic fractionation assays following combined OXA and HP treatment. (C) The effect of HP on Nrf2 protein expression was further examined by immunofluorescence. Scale bar, 50 μm. Data are expressed as mean ± standard deviation (n = 3); *$p < 0.05$, **$p < 0.01$, ***$p < 0.001$, and ****$p < 0.0001$.

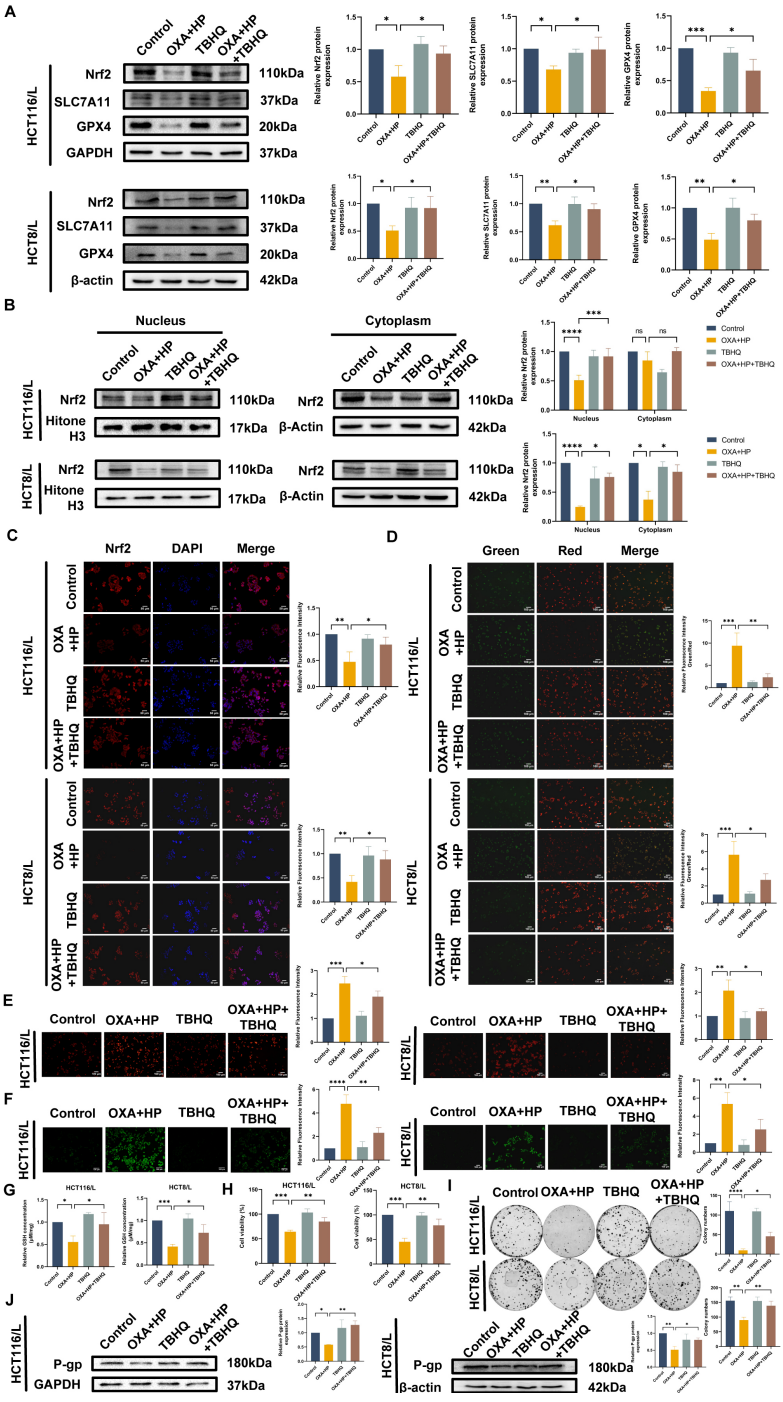

Fig. 7. Huaier polysaccharide (HP) enhances oxaliplatin (OXA) sensitivity by inducing ferroptosis via nuclear factor erythroid 2-related factor 2/solute carrier family 7 member 11/glutathione peroxidase (Nrf2/SLC7A11/GPX4) pathway suppression. (A) Protein expression levels of Nrf2, SLC7A11, and GPX4 in colorectal cancer drug-resistant cells treated with OXA combined with HP, with or without the Nrf2 activator tert-butylhydroquinone, were detected by western blotting. (B) The nuclear and cytoplasmic distribution of Nrf2 protein under the same treatment conditions was analyzed by nuclear–cytoplasmic fractionation. (C) The effect of HP on Nrf2 protein expression was further examined by immunofluorescence in similarly treated cells. Scale bar, 50 μm. (D) Lipid peroxide formation in colorectal cancer drug-resistant cells was assessed using the BODIPY 581/591 C11 fluorescent probe. Scale bar, 100 μm. (E) Intracellular Fe^{2+} levels were measured with FerroOrange. Scale bar, 100 μm. (F) Reactive oxygen species (ROS) levels in colorectal cancer drug-resistant cells were measured using a ROS assay kit. Scale bar, 100 μm. (G) Total glutathione (GSH) content was determined using a GSH assay kit. (H) Cell viability was evaluated by a Cell Counting Kit-8 assay. (I) Proliferative capacity was assessed using a colony formation assay. (J) P-glycoprotein (P-gp) protein expression levels were detected by western blotting. Data are expressed as mean ± standard deviation (n = 3). *$p < 0.05$, **$p < 0.01$, ***$p < 0.001$, and ****$p < 0.0001$; ns, not significant.

triple-negative breast cancer to immunotherapy by inhibiting cancer-associated fibroblasts [28], suppresses gastrointestinal stromal tumor proliferation and migration by modulating the JAK2/STAT3 pathway [29], and increases the chemosensitivity of hepatocellular carcinoma cells to OXA by downregulating YAP [30]. Despite its recognized antitumor, immunomodulatory, and chemosensitizing properties, the effects and molecular mechanisms of its key component (HP) on OXA chemosensitivity remain poorly understood. To our knowledge, this study is the first to investigate the role of HP in regulating the chemosensitivity of CRC cells to OXA *in vitro* and to elucidate the underlying molecular mechanisms. Our findings showed that HP inhibited the viability and proliferation of drug-resistant CRC cells and downregulated P-gp expression. These findings suggest that Huaier effectively enhances the sensitivity of drug-resistant CRC cells to OXA *in vitro* and that the combination of Huaier and OXA exerts a more pronounced synergistic effect.

Previous studies have reported that Huaier modulates ferroptosis in Panc-1 and MiaPaCa-2 pancreatic cancer cells by inducing autophagy-dependent ferroptosis, thereby inhibiting pancreatic cancer progression [31]. HP has also been shown to induce ferroptosis in MDA-MB-231 triple-negative breast cancer cells [32]. Based on these findings, we hypothesized that HP regulates ferroptosis in HCT116/L and HCT8/L cells. To test this hypothesis, ferroptosis in resistant cells was evaluated using transmission electron microscopy (TEM), the BODIPY 581/591 C11 fluorescent probe, the FerroOrange probe, a ROS assay, and a total GSH assay. HP treatment induced characteristic changes in ferroptosis, including mitochondrial shrinkage, increased lipid peroxidation, increased Fe^{2+} accumulation, increased ROS levels, and decreased total GSH levels, demonstrating that HP induces ferroptosis in HCT116/L cells.

To further determine whether HP overcomes OXA resistance by inducing ferroptosis, we performed the Fer-1 ferroptosis inhibitor test. Fer-1 significantly attenuated HP-induced ferroptosis, restored P-gp expression, and partially reversed cell viability suppression caused by HP. Collectively, these findings indicate that HP enhances OXA sensitivity by regulating ferroptosis.

We further investigated the mechanism by which HP enhances CRC cell sensitivity to OXA by inducing ferroptosis. Previous studies have suggested that the mechanism underlying HP-induced ferroptosis may involve Fe^{2+} accumulation, lipid peroxidation, and modulation of the p53/SLC7A11/GPX4 signaling axis [32]. In the present study, HP downregulated the protein expression of Nrf2, SLC7A11, and GPX4, indicating that HP suppresses the Nrf2/SLC7A11/GPX4 signaling pathway. Furthermore, treatment with the specific Nrf2 activator TBHQ combined with HP and OXA, TBHQ significantly reduced HP-induced ferroptosis, partially reversed P-gp downregulation, and restored cell viability. Collectively, these results indicate that HP enhanced the sensitivity of OXA-resistant CRC cells, primarily by inhibiting the Nrf2 pathway and activating ferroptosis.

The SLC7A11/GSH/GPX4 axis is a key cellular defense mechanism against ferroptosis and is closely associated with OXA resistance in CRC [9]. Nrf2, a master transcription factor that regulates redox homeostasis, is also implicated in this resistant phenotype [33]. Previous studies have shown that OXA promotes ferroptosis and oxidative stress in CRC cells by suppressing the Nrf2 signaling pathway [34].

To our knowledge, this study is the first to demonstrate that HP enhances the sensitivity of drug-resistant CRC cells to OXA *in vitro* by targeting and inhibiting the Nrf2/SLC7A11/GPX4 signaling pathway and inducing ferroptosis. This finding provides mechanistic evidence supporting the potential of HP to sensitize CRC cells to OXA and identifies a candidate target for natural product–based ferroptosis-inducing strategies. However, this study has several limitations. First, owing to the complexity of the multicomponent system in TCM, the synergistic mechanisms of other active components in Huaier warrant further investigation. The HP preparation used in this study contained flavonoids, phenolic acids, trace amounts of proteins/amino acids, and total polysaccharides, as described in the Materials and Methods section. Because further purification was not performed, these components may have influenced the experimental outcomes. Flavonoids and phenolic acids are known modulators of the Nrf2 signaling pathway and possess antioxidant activities that can synergize with or interfere with the regulatory effects of HP on the Nrf2/SLC7A11/GPX4 axis. In addition, amino acids such as cysteine may influence glutathione synthesis and consequently alter ferroptosis sensitivity. Therefore, the observed effects of HP on P-glycoprotein downregulation and ferroptosis induction cannot be attributed exclusively to the polysaccharide fraction. Further studies using highly purified polysaccharide fractions are needed to confirm the specificity of these findings. Second, the scope of experimental models should be expanded. Although the current study was performed only in cell-line models, future studies should include validation in animal models. Moreover, potential off-target effects and long-term safety of HP should be carefully evaluated. Although the literature suggests that HP exhibits minimal toxicity as evidenced by *in vitro, in vivo*, and clinical studies [20], providing preliminary support for its relatively safe biological profile, further systematic toxicological experiments and target screening are needed for any translational applications.

5. Conclusions

In summary, Huaier enhanced the sensitivity of chemoresistant CRC cells to OXA *in vitro* by suppressing the Nrf2/SLC7A11/GPX4 signaling axis, inducing ferroptosis, and downregulating P-gp expression. These findings

provide evidence supporting the role of Huaier in potentiating the efficacy of OXA-based chemotherapy.

Availability of Data and Materials

The data generated in the present study may be requested from the corresponding author.

Author Contributions

GW: Conceptualization, Validation, Formal analysis, Investigation, Writing - Original Draft, Writing - Review & Editing, Methodology. YY: Validation, Formal analysis. HJ: Methodology. XL and ZH provided assistance and advice for the Western Blot experiments. ZH was responsible for data analysis. JZ: Supervision, Project administration, Funding acquisition, Writing - Reviewing and Editing, designing the research study, making figures and tables, and searching for references. All authors contributed to editorial changes in the manuscript. All authors read and approved the final manuscript. All authors have participated sufficiently in the work and agreed to be accountable for all aspects of the work.

Ethics Approval and Consent to Participate

Not applicable.

Acknowledgment

Thanks to all the peer reviewers for their opinions and suggestions.

Funding

This work was supported by the Project Funding of Hebei Provincial Education Department [grant no. ZD2020137]; the Key Discipline Construction Project of Hebei Provincial Universities [grant no. Ji Jiao Gao 2013 (4) 2012 37].

Conflicts of Interest

The authors declare no conflicts of interest.

References

[1] Bray F, Laversanne M, Sung H, Ferlay J, Siegel RL, Soerjomataram I, et al. Global cancer statistics 2022: GLOBOCAN estimates of incidence and mortality worldwide for 36 cancers in 185 countries. CA: a Cancer Journal for Clinicians. 2024; 74: 229–263. https://doi.org/10.3322/caac.21834

[2] Cervantes A, Adam R, Roselló S, Arnold D, Normanno N, Taïeb J, et al. Metastatic colorectal cancer: ESMO Clinical Practice Guideline for diagnosis, treatment and follow-up. Annals of Oncology. 2023; 34: 10–32. https://doi.org/10.1016/j.annonc.2022.10.003

[3] Benson AB, Venook AP, Al-Hawary MM, Arain MA, Chen YJ, Ciombor KK, et al. Colon Cancer, Version 2.2021, NCCN Clinical Practice Guidelines in Oncology. Journal of the National Comprehensive Cancer Network. 2021; 19: 329–359. https://doi.org/10.6004/jnccn.2021.0012

[4] Yu T, An Q, Cao XL, Yang H, Cui J, Li ZJ, et al. GOLPH3 inhibition reverses oxaliplatin resistance of colon cancer cells via suppression of PI3K/AKT/mTOR pathway. Life Sciences. 2020; 260: 118294. https://doi.org/10.1016/j.lfs.2020.118294

[5] Dixon SJ, Lemberg KM, Lamprecht MR, Skouta R, Zaitsev EM, Gleason CE, et al. Ferroptosis: an iron-dependent form of nonapoptotic cell death. Cell. 2012; 149: 1060–1072. https://doi.org/10.1016/j.cell.2012.03.042

[6] Kong Z, Zhang M, Yuan H, Liu J, Sang H, Zhao P, et al. Exo-miR-1911-5p regulates ferroptosis to promote macrophages M2 polarization-mediated gastric cancer cisplatin resistance via MYB/AKR1B10/ACC. Communications Biology. 2025; 8: 1054. https://doi.org/10.1038/s42003-025-08441-w

[7] Li B, Wei Z, Wang Z, Xu F, Yang J, Lin B, et al. Fusobacterium nucleatum induces oxaliplatin resistance by inhibiting ferroptosis through E-cadherin/β-catenin/GPX4 axis in colorectal cancer. Free Radical Biology & Medicine. 2024; 220: 125–138. https://doi.org/10.1016/j.freeradbiomed.2024.04.226

[8] Zhang C, Liu X, Jin S, Chen Y, Guo R. Ferroptosis in cancer therapy: a novel approach to reversing drug resistance. Molecular Cancer. 2022; 21: 47. https://doi.org/10.1186/s12943-022-01530-y

[9] Zhong S, Wang Z, Yang J, Jiang D, Wang K. Ferroptosis-related oxaliplatin resistance in multiple cancers: Potential roles and therapeutic Implications. Heliyon. 2024; 10: e37613. https://doi.org/10.1016/j.heliyon.2024.e37613

[10] Rojo de la Vega M, Chapman E, Zhang DD. NRF2 and the Hallmarks of Cancer. Cancer Cell. 2018; 34: 21–43. https://doi.org/10.1016/j.ccell.2018.03.022

[11] Jayakumar S, Pal D, Sandur SK. Nrf2 facilitates repair of radiation induced DNA damage through homologous recombination repair pathway in a ROS independent manner in cancer cells. Mutation Research. 2015; 779: 33–45. https://doi.org/10.1016/j.mrfmmm.2015.06.007

[12] Gong D, Chen M, Wang Y, Shi J, Hou Y. Role of ferroptosis on tumor progression and immunotherapy. Cell Death Discovery. 2022; 8: 427. https://doi.org/10.1038/s41420-022-01218-8

[13] Pan J, Yang C, Jiang Z, Huang J. Trametes robiniophila Murr: a traditional Chinese medicine with potent anti-tumor effects. Cancer Management and Research. 2019; 11: 1541–1549. https://doi.org/10.2147/CMAR.S193174

[14] Wang Z, Yu XL, Zhang J, Cheng ZG, Han ZY, Liu FY, et al. Huaier granule prevents the recurrence of early-stage hepatocellular carcinoma after thermal ablation: A cohort study. Journal of Ethnopharmacology. 2021; 281: 114539. https://doi.org/10.1016/j.jep.2021.114539

[15] Li C, Wang X, Chen T, Wang W, Yang Q. Trametes robiniophila Murr in the treatment of breast cancer. Biomedicine & Pharmacotherapy. 2020; 128: 110254. https://doi.org/10.1016/j.biopha.2020.110254

[16] Chen J, Li Y, Sun Q, Wang Y, Qiu Z, He X, et al. Huaier overcomes tumor-induced immunosuppression in colorectal cancer by activating MHC I and CD8+ T cells. Phytomedicine : international journal of phytotherapy and phytopharmacology. 2025; 147: 157157. https://doi.org/10.1016/j.phymed.2025.157157

[17] Yang L, Song Z, Wang X, Yang W, Wang M, Liu H. Huaier extract enhances the treatment efficacy of paclitaxel in breast cancer cells via the NF-κB/IκBα pathway. Oncology Reports. 2017; 38: 3455–3464. https://doi.org/10.3892/or.2017.6024

[18] Jin H, Liu C, Liu X, Wang H, Zhang Y, Liu Y, et al. Huaier suppresses cisplatin resistance in non-small cell lung cancer by inhibiting the JNK/JUN/IL-8 signaling pathway. Journal of Ethnopharmacology. 2024; 319: 117270. https://doi.org/10.1016/j.jep.2023.117270

[19] Li X, Zhang H, Deng Y, Fang Q, Zhang X, Ding S, et al. Huaier polysaccharides inhibits hepatocellular carcinoma via gut microbiota mediated M2 macrophage polarization. International Jour-

nal of Biological Macromolecules. 2025; 293: 139357. https://doi.org/10.1016/j.ijbiomac.2024.139357

[20] Long H, Wu Z. Immunoregulatory effects of Huaier (Trametes robiniophila Murr) and relevant clinical applications. Frontiers in Immunology. 2023; 14: 1147098. https://doi.org/10.3389/fimmu.2023.1147098

[21] Wang Y, Liu Y, Hu Y. Optimization of polysaccharides extraction from Trametes robiniophila and its antioxidant activities. Carbohydrate Polymers. 2014; 111: 324–332. https://doi.org/10.1016/j.carbpol.2014.03.083

[22] Xi Y, Xu P. Global colorectal cancer burden in 2020 and projections to 2040. Translational Oncology. 2021; 14: 101174. https://doi.org/10.1016/j.tranon.2021.101174

[23] Huang CZ, Zhou Y, Tong QS, Duan QJ, Zhang Q, Du JZ, et al. Precision medicine-guided co-delivery of ASPN siRNA and oxaliplatin by nanoparticles to overcome chemoresistance of colorectal cancer. Biomaterials. 2022; 290: 121827. https://doi.org/10.1016/j.biomaterials.2022.121827

[24] Yang J, Lin D, Huang Y, Yin S, Chen M, Sun H, et al. Clock gene ARNTL2 enhances 5-fluorouracil resistance in colon cancer by upregulating SLC7A11 to suppress ferroptosis. Redox Biology. 2025; 86: 103798. https://doi.org/10.1016/j.redox.2025.103798

[25] Khan S, Karmokar A, Howells L, Britton RG, Parrott E, Palacios-Gallego R, et al. An old spice with new tricks: Curcumin targets adenoma and colorectal cancer stem-like cells associated with poor survival outcomes. Cancer Letters. 2025; 629: 217885. https://doi.org/10.1016/j.canlet.2025.217885

[26] Lin X, Xu L, Gu M, Shao H, Yao L, Huang X. Gegen Qinlian Decoction reverses oxaliplatin resistance in colorectal cancer by inhibiting YTHDF1-regulated m6A modification of GLS1. Phytomedicine. 2024; 133: 155906. https://doi.org/10.1016/j.phymed.2024.155906

[27] Li B, Cao Q, Liu Z. The treatment effects of Trametes Robiniophila Murr against colorectal cancer: A mini-review. Frontiers in Medicine. 2022; 9: 981516. https://doi.org/10.3389/fmed.2022.981516

[28] Li C, Wang X, Xing L, Chen T, Li W, Li X, et al. Huaier-induced suppression of cancer-associated fibroblasts confers immunotherapeutic sensitivity in triple-negative breast cancer. Phytomedicine : International Journal of Phytotherapy and Phytopharmacology. 2024; 135: 156051. https://doi.org/10.1016/j.phymed.2024.156051

[29] Cao L, Li Z, Huang Y, Chen H, Chen L, Tao L, et al. Huaier inhibits the proliferation and migration of gastrointestinal stromal tumors by regulating the JAK2 / STAT3 signaling pathway. Journal of Ethnopharmacology. 2025; 342: 119389. https://doi.org/10.1016/j.jep.2025.119389

[30] Tao Y, Shan L, Xu X, Jiang H, Chen R, Qian Z, et al. Huaier Augmented the Chemotherapeutic Sensitivity of Oxaliplatin via Downregulation of YAP in Hepatocellular Carcinoma. Journal of Cancer. 2018; 9: 3962–3970. https://doi.org/10.7150/jca.25909

[31] Zhu Z, Wang X, Zhang W, Gong M, Zhang S, Yang B, et al. Huaier suppresses pancreatic cancer progression via activating cell autophagy induced ferroptosis. Frontiers in Oncology. 2022; 12: 960858. https://doi.org/10.3389/fonc.2022.960858

[32] Wang L, Gao X, Gao S, Wang T, Feng X, Wang Y, et al. Mechanism of Trametes robiniophila polysaccharide-induced ferroptosis in triple-negative breast cancer MDA-MB-231 cells. Zhong Yi Yao Dao Bao. 2025; 31: 47–52. https://doi.org/10.13862/j.cn43-1446/r.2025.08.008. (In Chinese).

[33] Hayes JD, Dinkova-Kostova AT. The Nrf2 regulatory network provides an interface between redox and intermediary metabolism. Trends in Biochemical Sciences. 2014; 39: 199–218. https://doi.org/10.1016/j.tibs.2014.02.002

[34] Liu B, Wang H. Oxaliplatin induces ferroptosis and oxidative stress in HT29 colorectal cancer cells by inhibiting the Nrf2 signaling pathway. Experimental and Therapeutic Medicine. 2022; 23: 394. https://doi.org/10.3892/etm.2022.11321